JETIR.ORG ISSN: 2349-5162 | ESTD Year : 2014 | Monthly Issue
JOURNAL OF EMERGING TECHNOLOGIES AND INNOVATIVE RESEARCH (JETIR)
An International Scholarly Open Access, Peer-reviewed, Refereed Journal

SYNTHESIS AND CHARACTERIZATION OF ORGANIC SOLAR CELL

[1] Madavi Shekar, [2] Dr. K. Srinivasa Reddy
[1 & 2] Department of Physics,
[1 & 2] JNTUH University of Engineering, Science and Technology Hyderabad,
Kukatpally, Hyderabad -500085.

Abstract: In this work, ZnO and SnO_2 are used as electron transport layers (ETLs) in organic solar cells (OSCs) to synthesize and characterize them under ambient circumstances. ZnO and SnO_2 thin films were created using the spin-coating technique, and their optical and structural characteristics were examined under a range of conditions, including annealing time and temperature. The production of crystalline ZnO and SnO_2, which are necessary for efficient charge transfer in OSCs, was verified by X-ray diffraction (XRD). Compared to traditional OSC designs, the constructed OSCs showed improved stability and efficiency in inverted topologies, particularly when using ZnO as the ETL. The results highlight how crucial material choice and environmental stability are to enhancing OSC performance and lifetime and increasing their viability for commercial use. By highlighting long-lasting material combinations for workable energy solutions and improving fabrication conditions, this research advances OSC technology.

Key Words: X-ray diffraction (XRD), ZnO, SnO_2, Electron transport layer (ETLs).

1. Introduction

The evolution of organic solar cells (OSCs) represents a fascinating journey marked by significant milestones and innovations that reflect the interplay between organic chemistry, materials science, and the increasing global focus on renewable energy. Starting in the mid-20th century, initial explorations laid the groundwork for understanding the electrical properties of organic materials, leading to the discovery that these substances could conduct electricity under light exposure, albeit with limited effectiveness as photovoltaic materials [1]. As research progressed into the 1980s and 1990s, the landscape of OSCs transformed with breakthroughs in conjugated polymers and fullerene-based acceptors. This period saw the emergence of more efficient organic materials, which were critical for enhancing the performance of solar cells. A pivotal moment came with the introduction of bulk heterojunction (BHJ) solar cells at the turn of the millennium, where the innovative mixing of donor and acceptor materials dramatically improved charge separation and transport, paving the way for higher efficiencies [2, 3]. The classification of organic solar cells is multifaceted, ranging In the 2010s, the focus shifted towards non-fullerene acceptors (NFAs), which offered tunable electronic properties that significantly enhanced device performance. This era marked a key transition as researchers sought to develop OSCs that could compete with traditional inorganic solar technologies in terms of efficiency and stability. The 2020s continued this trend with advancements in tandem organic solar cells, which stack multiple layers to capture a wider spectrum of sunlight, further pushing the boundaries of efficiency [4, 5].

2. Literature Review

Organic solar cells (OSCs) are increasingly favored for their cost-effectiveness and flexibility, thanks to their solution-based fabrication processes that enable large-area and roll-to-roll manufacturing. The introduction of non-fullerene acceptors has significantly boosted power conversion efficiencies (PCEs), with recent studies reporting values over 18% (Li et al., 2020) [6]. The active layer of OSCs typically combines a conjugated polymer donor with an electron acceptor material, where the morphology of this layer is critical for device efficiency. Zhang et al. (2021) highlighted that optimizing the donor-acceptor interface enhances charge separation and transport, leading to better performance [7]. Characterization techniques, such as UV-vis spectroscopy and cyclic voltammetry, are essential for evaluating the optical and electronic properties of OSC materials. UV-vis spectroscopy, in particular, is crucial for assessing light absorption, which is vital for optimizing active layer composition (Kumar and Bhanja, 2019) [8]. Stability under operational conditions is another key factor for the commercial viability of OSCs. Chen et al. (2022) noted that optimized encapsulation and stable materials can significantly prolong device lifespan, especially under thermal and light stress [9]. Energy level alignment between donor and acceptor materials is crucial for maximizing charge extraction. Wang et al. (2020) found that fine-tuning the energy levels through polymer substituents can enhance open-circuit voltage and overall efficiency [10]. Additionally, the choice of solvent during solution processing can greatly influence active layer morphology, affecting charge transport properties (Park et al., 2018) [11]. The incorporation of nanomaterials, like silver nanoparticles, can further enhance OSC performance by improving light harvesting and charge transport (Lee et al., 2019) [12].

3. Methodology

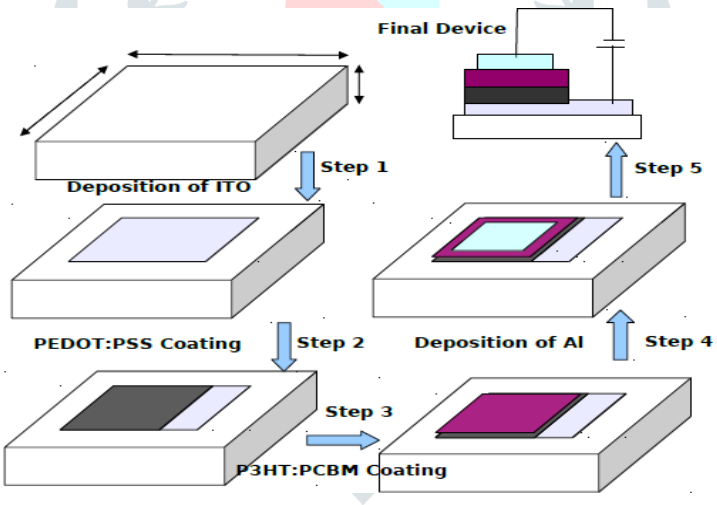

Figure (1): Spin Coating method

Step 1: Indium Tin Oxide (ITO) Deposition

The process begins with the deposition of a transparent conductive film of Indium Tin Oxide (ITO) on a substrate, which may be glass or plastic. The ITO layer serves as the anode, enabling light transmission while conducting electricity. The ITO is applied using a magnetron sputtering system, operated at an initial vacuum pressure of 4.0×10^{-5} Torr and 40 W RF power. This setup creates a vacuum in the chamber, followed by a sputtering process that deposits a nominal thickness of 200 nm over approximately 1 hour and 8 minutes, with careful monitoring using a thickness gauge.

Step 2: PEDOT: PSS Layer Application

Once the ITO layer is in place, a conductive polymer layer of PEDOT: PSS is applied to enhance hole mobility and improve device efficiency. The PEDOT: PSS solution is filtered through a 0.2 µm mesh and then deposited using a spin coater. The process begins by applying drops of the solution to the glass surface in

dynamic dispense mode at 200 rpm for 10 seconds. Subsequently, the sample undergoes a thinning process at a high-speed of 1000 rpm for 40 seconds, achieving an optimized thickness of 50 nm on flat glass slides before applying it to the ITO-coated substrates.

Step 3: Coating with P3HT: PCBM Blend

The next step involves the deposition of the active layer, created by blending P3HT (polymer electron donor) and PCBM (fullerene electron acceptor). A 1 wt% solution with a 1:1 ratio of P3HT and PCBM is prepared by mixing 11.11 mg/ml of each component and stirring the mixture at 50°C for 12 hours. The optimized solution is then spin-coated onto the PEDOT: PSS/ITO-coated substrate at 1500 rpm for 45 minutes, resulting in a layer approximately 100 nm thick, responsible for light absorption and charge carrier generation.

Step 4: Aluminum Cathode Deposition

To form the cathode, a thin film of aluminum is deposited over the active layer using thermal vacuum evaporation. The deposition rate and thickness are carefully controlled using the Infineon Thin Film Controller. The aluminum layer is applied through a shadow mask to create the necessary back contact for electron collection from the P3HT: PCBM layer.

Step 5: Final Device Formation

At this stage, the organic solar cell is fully constructed with all layers in place. The final device is now ready for photovoltaic applications, capable of converting light into electrical energy.

Additional Steps: Glass Slide Preparation

Before the deposition processes, glass slides are meticulously prepared. The work table is cleaned with ethanol, and glass slides are cut into 1 cm^2 squares. They are thoroughly washed in deionized water, soaked in acetone, and cleaned in an ultrasonic cleaner for 10 minutes at room temperature. Finally, the slides are blow-dried using nitrogen gas to ensure a contaminant-free surface for optimal layer adhesion.

4. Results and Discussion

4.1. XRD Pattern of ZnO:

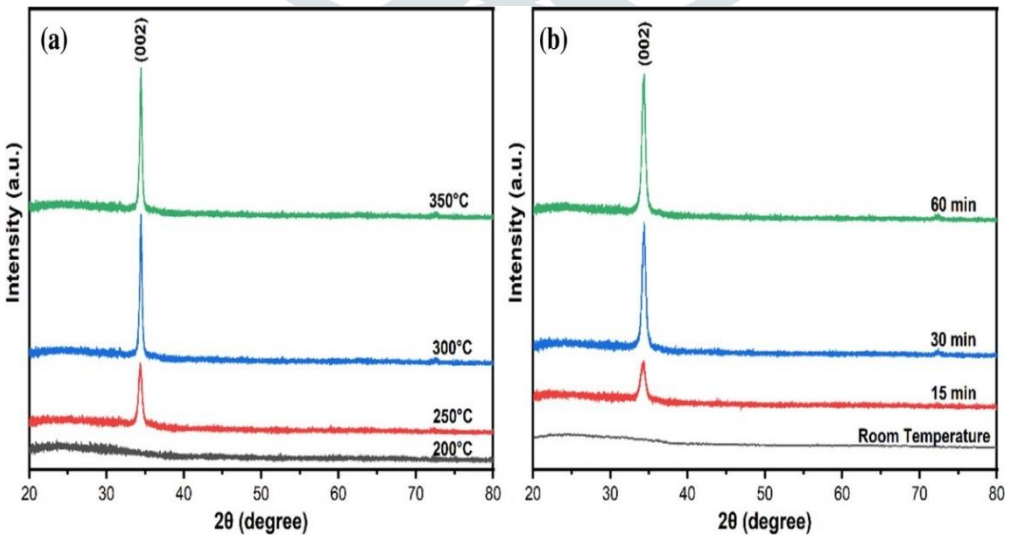

Figure (2): XRD pattern of ZnO thin films grown at
(a) different temperatures and (b) different duration of growth at 300°C for 0.1 M.

The X-ray diffraction (XRD) patterns of ZnO thin films are profoundly affected by both the growth temperature and duration, which play crucial roles in determining their structural characteristics, such as crystallinity, orientation, and grain size. At lower growth temperatures, the resulting ZnO films typically display poor crystallinity, evidenced by broader XRD peaks. This broadening indicates smaller crystallite sizes and a lack of distinct crystal planes, with key peaks associated with the wurtzite structure like (100), (002), and (101)—being weak, signifying inadequate preferential alignment. As the growth temperature increases to intermediate levels, there is a notable enhancement in crystallinity, leading to sharper and more pronounced peaks in the XRD patterns. The (002) peak, in particular, becomes more prominent, suggesting that the ZnO films grow preferentially with their c-axis oriented perpendicular to the substrate, which is a desirable trait for many applications. At high temperatures, the films exhibit superior crystallinity characterized by narrower peaks due to larger grain sizes and well-defined orientations.

However, it is important to note that excessively high temperatures can introduce defects and mechanical stress, potentially resulting in peak shifts or the emergence of additional peaks, although the (002) peak generally remains strong. Optimal growth temperatures, usually in the range of 300°C to 400°C, produce sharp XRD peaks corresponding to the (002) plane, indicating well-crystallized and oriented films. In terms of growth duration at a constant temperature of 300°C, shorter growth periods yield films with smaller grains, leading to broader peaks and less distinct (002) peaks, which point to incomplete c-axis growth. As the growth duration increases to moderate levels, the films demonstrate improved crystallinity, as indicated by narrower peaks and enhanced intensity of the (002) peak, reflecting better alignment along the c-axis. Conversely, if the growth duration is extended excessively, it may result in further narrowing of the peaks, but this can also induce stress and defects, causing peak broadening or the appearance of additional peaks.

Moreover, overly thick films run the risk of cracking, which negatively affects the overall XRD pattern. Overall, there is a clear correlation between higher temperatures and longer growth durations with sharper and more intense peaks, particularly for the (002) plane, which serves as a strong indicator of improved crystalline quality in ZnO thin films.

4.2. XRD pattern of SnO_2:

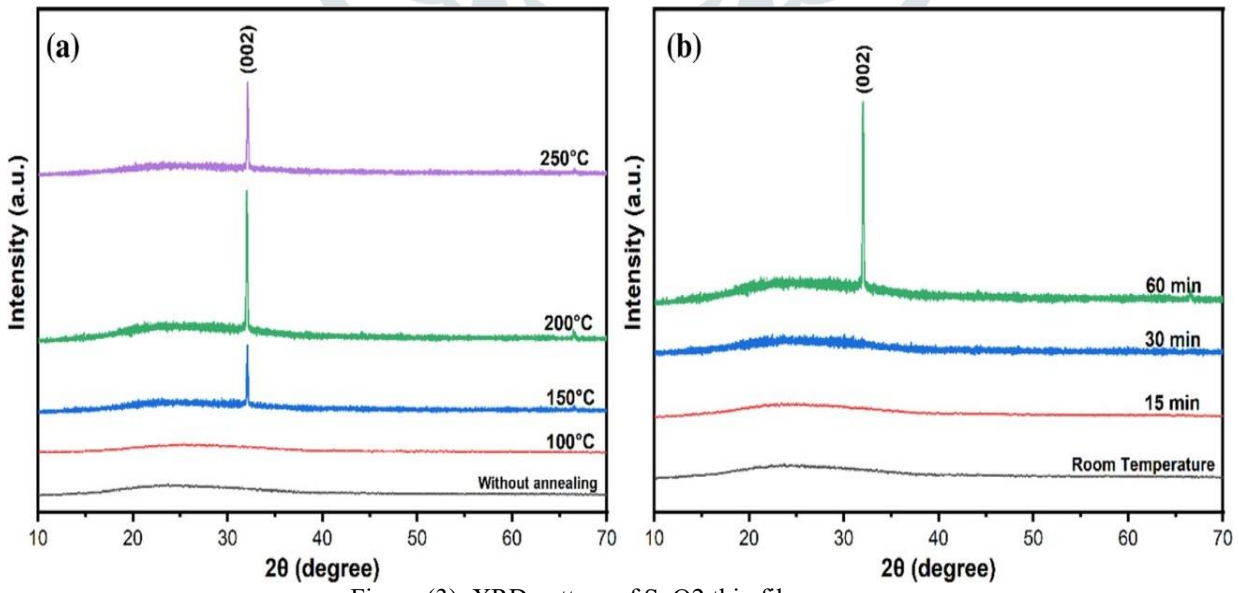

Figure (3): XRD pattern of SnO2 thin films grown
(a) at different temperatures and (b) at 200°C for different annealing durations using 0.1 M SnCl2.

The X-ray diffraction (XRD) patterns of SnO_2 thin films reveal critical information about their crystalline structure, particularly the behaviour of the (002) peak under various conditions of temperature and annealing time. For films deposited at temperatures of 100°C, 150°C, 200°C, and 250°C, the XRD profiles

indicate significant variations in crystallinity. The unannealed sample shows minimal diffraction peaks, suggesting it is mostly amorphous. At 100°C, the (002) peak begins to emerge, indicating initial crystallization, while at 150°C, this peak becomes more pronounced, marking a transition to a more crystalline phase. By 200°C, the (002) peak sharpens, indicating the formation of a well-ordered SnO_2 phase, with crystallinity stabilizing at this temperature, as no significant improvement is observed at 250°C.

In summary, crystallinity improves with temperature, peaking at 200°C, while lower temperatures yield largely amorphous films. Furthermore, when examining the effects of annealing duration at 200°C, it was found that a room temperature sample and a 15-minute annealed sample both show weak or no significant peaks, suggesting an amorphous state. However, after 30 minutes of annealing, the (002) peak becomes more defined, and at 60 minutes, it reaches maximum intensity, indicating optimal crystallization. Thus, the annealing duration greatly affects the crystallinity of SnO_2 films, with 60 minutes at 200°C yielding the most well-crystallized structure.

4.3. Characterization of UV-Visible Spectrum

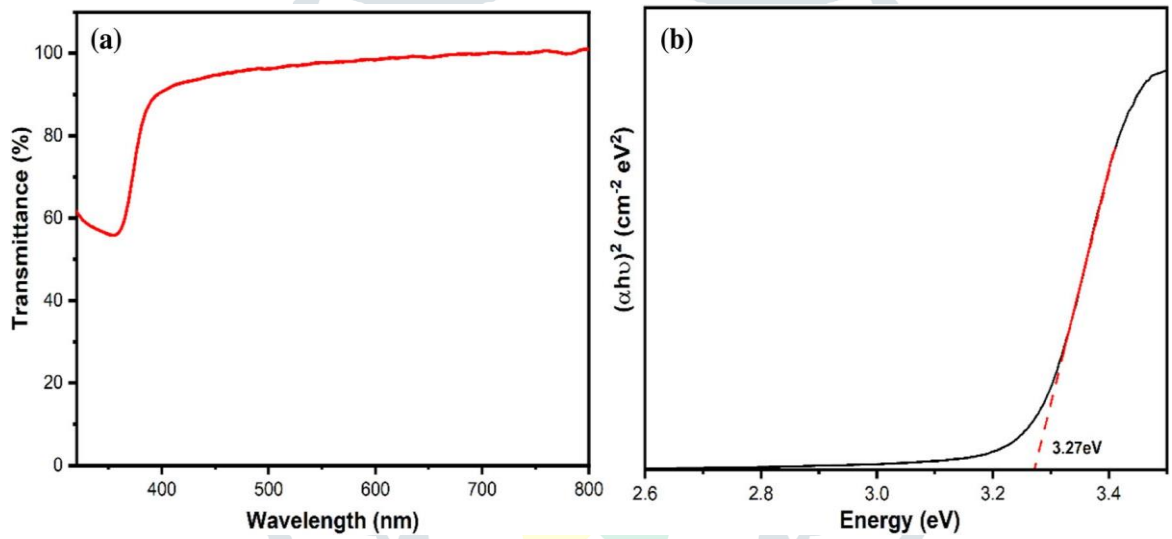

Figure (4): (a) UV–vis transmittance spectrum and (b) Tauc plot of ZnO thin film grown at 300°C

The optical properties of a ZnO thin film grown at 300°C are illustrated through the UV–vis transmittance spectrum and the Tauc plot. The UV–vis spectrum reveals that the film initially shows around 60% transmittance in the ultraviolet range, with a sharp increase to approximately 90-100% transmittance between 400-800 nm in the visible spectrum. This indicates that ZnO is highly transparent in the visible range while effectively absorbing UV light, making it suitable for optoelectronic applications and UV filtering. The Tauc plot, which relates the square of the absorption coefficient (α) to photon energy (hv), is used to determine the optical bandgap. By applying a linear fit to the high-energy region of the plot, the optical bandgap is estimated to be around 3.27 eV, aligning with the expected value for ZnO.

These analyses are crucial for characterizing semiconductor thin films, providing insights into their transparency and optical bandgap, which are essential for evaluating ZnO's applicability in advanced electronic and photonic devices. Together, the UV–vis spectrum and Tauc plot underscore the film's effective UV absorption and suitable optical bandgap, highlighting ZnO's potential in various material applications.

4.4. UV–vis absorption spectra of the P3HT: PCBM thin films on different electron transport layers

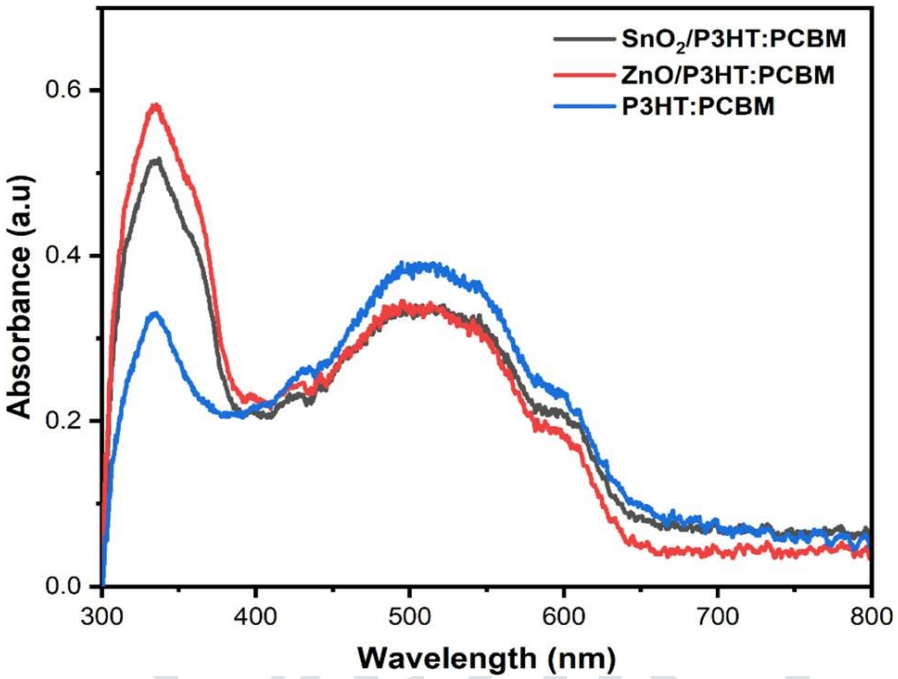

Figure (5): UV–vis absorption spectra of the P3HT: PCBM thin films on different electron transport layers.

The UV-Vis absorption spectrum analyzes how different electron transport layers (ETLs) affect the absorbance of P3HT thin films. The SnO_2/P3HT configuration (black curve) shows lower absorbance compared to other ETLs, with moderate peaks around 330 nm and 500 nm, indicating less effective light absorption and suggesting that SnO_2 may not optimize light harvesting. In contrast, the ZnO/P3HT configuration (red curve) exhibits significantly higher absorbance, particularly in the UV region at around 330 nm, with a broader and more pronounced absorption peak between 500-600 nm.

This indicates that ZnO enhances the film's overall light absorption capabilities, improving the interaction between light and the P3HT layer for better performance. The bare P3HT film (blue curve) demonstrates generally lower absorbance throughout the spectrum, with a noticeable peak near 500 nm, typical for P3HT, but significantly less absorption in the UV range compared to the ZnO/P3HT configuration. Overall, the spectrum highlights the importance of the ETL choice on the optical absorption properties of P3HT films, with ZnO proving to be a more efficient option for applications such as organic photovoltaics by maximizing light absorption and potentially increasing energy conversion efficiencies.

4.5. J-V Characteristics of the Organic Solar Cell with different cell configurations:

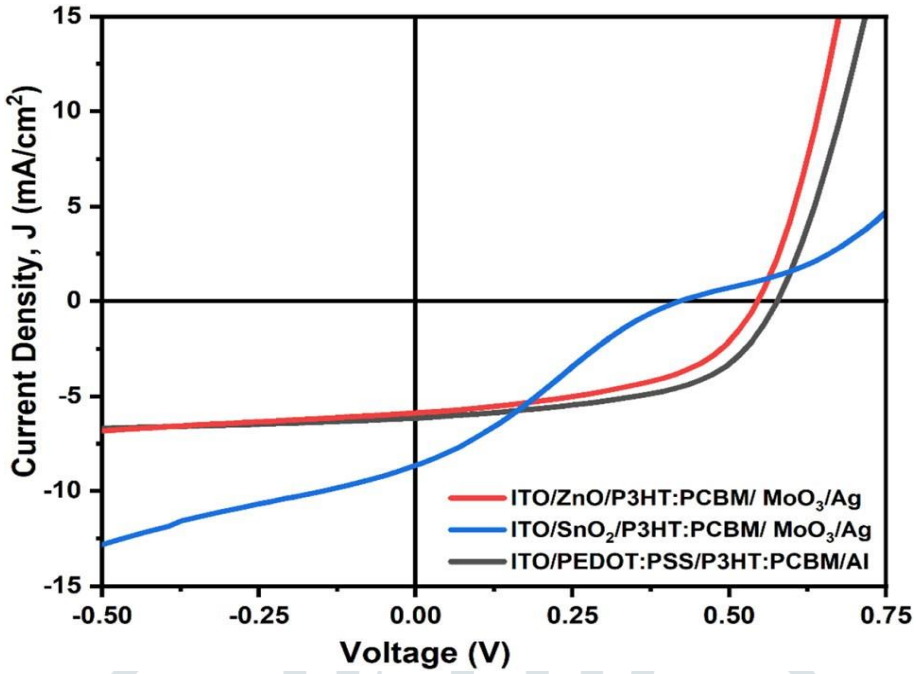

Figure (6): J-V Characteristics of the Organic Solar Cell with different cell configurations
Current Density vs. Voltage Characteristics of Organic Solar Cells

The graph presents the current density versus voltage (J-V) behaviour of three types of photovoltaic devices, each with different electron transport layers (ETLs) and cathode materials. The devices all use a P3HT, active layer, but vary in their ETLs: one uses ZnO (red curve), another uses SnO_2 (blue curve), and the third uses PEDOT (gray curve). Each ETL impacts the device's performance, with ZnO and PEDOT devices generally showing higher current density and a sharper increase in current at positive voltages, which suggests stronger rectification behaviour and potentially better efficiency. The SnO_2 device, on the other hand, shows a lower current density across the voltage range and a more gradual curve, indicating different electronic properties and possibly less efficient charge transport.

The cathode materials also differ among the devices, with ZnO and SnO_2 devices utilizing MoO_3/Ag, while the PEDOT. This difference in materials likely contributes to variations in the devices' current output and overall performance. From around 0.3 V to 0.75 V, the ZnO and PEDOT devices exhibit a more rapid rise in current density compared to the SnO_2 device, highlighting the influence of ETL and cathode choice on photovoltaic performance. The steep slope at higher voltages for ZnO and PEDOT devices implies reduced resistance and efficient charge collection, enhancing overall device efficiency.

In contrast, the SnO_2 device's gentler slope reflects less efficient charge extraction or transport. This analysis emphasizes that both ETL and cathode materials play crucial roles in optimizing photovoltaic device performance, impacting parameters like current density, charge transport, and rectification.

4.6. J–V characteristics of the OSCs with different cell configurations after keeping the devices in ambient conditions for 24 h.

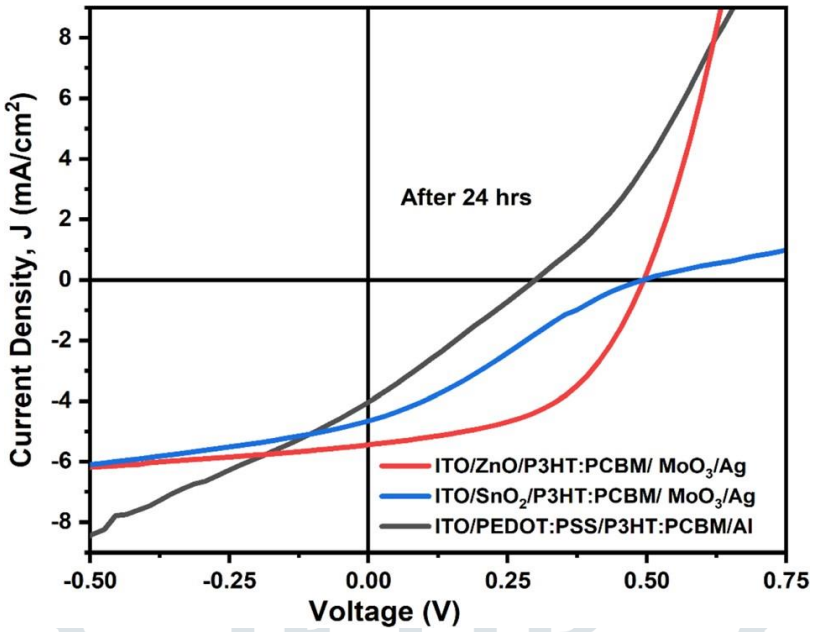

Figure (7): J–V characteristics of the OSCs with different cell configurations after keeping the devices in ambient conditions for 24 h.

The graph illustrates the current density (J) versus voltage (V) characteristics of organic solar cells (OSCs) with three different configurations after 24 hours in ambient conditions, evaluating their stability and performance under environmental exposure. The x-axis represents the applied voltage in volts, while the y-axis shows current density in mA/cm², indicating the generated current per unit area. The configurations include ITO/ZnO/P3HT: PCBM/MoO_3/Ag (red curve), ITO/SnO_2/P3HT: PCBM/MoO_3/Ag (blue curve), and ITO/PEDOT: PSS/P3HT: PCBM/Al (black curve).

Key performance metrics include short-circuit current density (Jsc) at zero voltage, open-circuit voltage (Voc) where current density is zero, and fill factor (FF), which indicates the curve's shape and efficiency. The ITO/PEDOT: PSS configuration (black) maintains the highest current density, suggesting the best stability and power retention. The ITO/ZnO device (red) shows moderate stability but some degradation, while the ITO/SnO_2 device (blue) displays the lowest performance, indicating higher susceptibility to environmental degradation.

5. Conclusion:

This study showed that ZnO-configured organic solar cells (OSCs) offer improved stability and efficiency, particularly in the presence of ambient air. Comparative investigation of several ETL materials revealed that ZnO-based designs maintained superior performance, but SnO_2-based cells are more prone to degradation. The study also demonstrated that inverted OSCs are more durable than traditional designs, highlighting the significance of ETL selection and structural orientation. These findings provide insights into material and structural optimization to improve OSC durability and efficiency, supporting the continued development of ZnO-based OSCs for sustainable energy applications.

.

Reference:

1. J. C. Hummelen, et al. "The synthesis of soluble methanofullerene derivatives for use in plastic solar cells." Chemical Communications (1995): 19-20.
2. A. J. Heeger. "Semiconducting polymers: the third generation." Proceedings of the National Academy of Sciences (2001): 1749-1751.
3. C. W. Tang. "Two-layer organic photovoltaic cell." Applied Physics Letters (1986): 220-222.
4. Y. Zhang, et al. "Recent progress in non-fullerene organic solar cells." Advanced Energy Materials (2018): 1702957.
5. J. Liu, et al. "Tandem organic solar cells with a high fill factor." Nature Communications (2019): 10, 1-8.
6. Li, Y., et al. (2020). "Recent Advances in Non-Fullerene Organic Solar Cells." Advanced Materials, 32(8), 1907443.
7. Zhang, Y., et al. (2021). "Molecular Engineering of Donor–Acceptor Interfaces for High-Performance Organic Solar Cells." Nature Energy, 6(1), 51-58.
8. Kumar, S., & Bhanja, P. (2019). "Characterization of Organic Solar Cells: A Review." Materials Today: Proceedings, 19, 763-767.
9. Chen, H., et al. (2022). "Improving Stability of Organic Solar Cells: Recent Advances and Future Directions." Energy & Environmental Science, 15(2), 483-507.
10. Wang, F., et al. (2020). "Tuning Energy Levels of Organic Semiconductors for High-Performance Solar Cells." Advanced Energy Materials, 10(15), 1903834.
11. Park, J. H., et al. (2018). "Solvent Effects on the Morphology and Performance of Organic Photovoltaics." Journal of Materials Chemistry A, 6(20), 9347-9355.
12. Lee, K., et al. (2019). "Enhancing Organic Solar Cell Performance Using Silver Nanoparticles." Solar Energy Materials and Solar Cells, 203, 110142.